Applied Catalysis B: Environmental 301 (2022) 120808

Contents lists available at ScienceDirect

Applied Catalysis B: Environmental

journal homepage: www.elsevier.com/locate/apcatb

Localized surface plasmon resonance enhanced electrochemical nitrogen reduction reaction

Wenkai Liang [a,1], Wei Qin [a,1], Dong Li [a,1], Yawen Wang [a], Wei Guo [a], Yuanting Bi [a], Yinghui Sun [b,*], Lin Jiang [a,*]

[a] Institute of Functional Nano & Soft Materials Laboratory (FUNSOM), Jiangsu Key Laboratory for Carbon-Based Functional Materials & Devices, Soochow University, Suzhou 215123, China

[b] College of Energy, Soochow Institute for Energy and Materials Innovations, Key Laboratory of Advanced Carbon Materials and Wearable Energy Technologies of Jiangsu Province, Soochow University, Suzhou 215006, China

ARTICLE INFO

Keywords:
Localized surface plasmon resonance (LSPR)
Electrochemical nitrogen reduction reaction (ENRR)
Electrocatalysts
Hot electrons
Au nanorods (Au NRs)

ABSTRACT

Localized surface plasmon resonance (LSPR) can effectively improve the catalytic activity of electrocatalysts by using solar energy. However, the application of LSPR effect in the electrochemical nitrogen reduction reaction (ENRR) is still blank and the ability of LSPR to enhance the catalytic activity of ENRR is unclear. Herein, the effective enhancement for the NRR electrocatalytic activity of Au nanorods (NRs) under illumination conditions based on the LSPR effect was successfully achieved. Under the irradiation of 808 nm laser (80 mW cm^{-2}), the rate of ammonia yield increased about 63.6% with comparison of that in dark. Meanwhile, combined with the results of the Finite difference time domain method (FDTD) simulation and photocurrent analysis, it is proved that the hot electrons excited by LSPR effect can effectively promote the ENRR catalytic activity of Au NRs. This study provides an important reference for the design of a novel LSPR-promoted electrocatalyst for NRR.

1. Introduction

Solar energy is the cleanest and most abundant renewable energy source available [1–5], and how to efficiently capture and convert solar energy and extend the application in energy utilization and chemical production are still being pursued. Plasmonic metal nanoparticles (such as Au, Ag, and Cu), which exhibit strong localized surface plasmon resonance (LSPR) properties, can efficiently enhance the sunlight harvesting ability, thereby becoming the focus of research in recent years [6–13]. The LSPR occurs when a nanoparticle with high free-electron mobility interacts with photons those match the resonance energy of the collective oscillation of the surface valence electrons. Then, a strong electromagnetic field forms on the surface of the nanoparticles and further decays to form high-energy electrons (hot electrons) between the vacuum energy and the Fermi level [14,15]. Hot electrons can be directly injected into the anti-bonding orbitals of the reactive molecules adsorbed on the surface of the nanostructure, reducing the activation energy, promoting the initiation of chemical reactions, and effectively enhancing the chemical reaction activity [6,10,11,16–24].

Recent studies have proved that applying the LSPR effect of metal nanoparticles into traditional electrocatalytic systems can change the catalytic reaction path and improve the catalytic efficiency and selectivity of electrocatalyst itself [25–28]. For example, the hot electrons excited by LSPR of Ag-Pt nanocages can inhibit the formation of peroxide intermediates in the oxygen reduction reaction (ORR) process [26]. Moreover, the catalytic activity and selectivity of the silver thin film electrode in the carbon dioxide reduction reaction (CO_2RR) also can be regulated under the effect of LSPR [28]. Therefore, solar energy can be maximized to effectively improve the catalytic activity of the electrocatalyst based on the unique LSPR effect of metal nanostructures. The electrochemical nitrogen reduction reaction (ENRR) has gradually become the focus of research due to the lower energy requirements and no greenhouse gas emissions compared with the traditional ammonia (NH_3) production [29–40]. However, the slow and complex reaction process of nitrogen (N_2) on the ENRR catalyst surface severely limits the final catalytic efficiency, which is far below the requirements for industrial production [41,42]. Meanwhile, it has been proved that the LSPR effect can effectively enhance the catalytic activity of the catalyst

* Corresponding authors.
E-mail addresses: yinghuisun@suda.edu.cn (Y. Sun), ljiang@suda.edu.cn (L. Jiang).
[1] These authors contributed equally.

https://doi.org/10.1016/j.apcatb.2021.120808
Received 21 June 2021; Received in revised form 30 August 2021; Accepted 7 October 2021
Available online 15 October 2021

in the photocatalytic NRR, indicating that LSPR has the possibility of application in the ENRR reaction [14,43,44]. If the LSPR effect of metal nanostructures can be incorporated into the ENRR reaction system, it is very feasible to use the hot electrons to effectively enhance the NRR catalytic efficiency of metal nanostructures itself and achieve improved ammonia yield rate. However, there is no research report on the utilization of LSPR effect to enhance the electrocatalytic NRR performance as far as we know. The enhancing ability of LSPR on the catalytic activity of ENRR is still unclear and needs to be further explored.

Here, the LSPR effect from Au nanorods (NRs) - based electrocatalyst was used to successfully achieve the effective enhancement of the ENRR activity of Au NRs itself under illumination condition. The electrode was prepared by drip coating the solution of Au NRs with naphthol on carbon paper, which could effectively avoid the aggregation of Au NRs and maintain the LSPR properties. With the assistance of 808 nm laser (80 mW cm^{-2}), the ammonia yield rate of Au NRs electrode is increased by about 63.6%. Meanwhile, compared with dark conditions, the increase of ammonia yield rate under illumination condition is much greater than that of hydrogen yield rate in the same test system, further proving that the illumination exhibits a better promoting effect on ENRR. Under the irradiation of the 808 nm laser, the ratio of the rapid-response current (I_{rapid}) to the total response photocurrent (I_{Total}, I_{Rapid}/I_{Total}) reaches the maximum value (37.43%), which means that more hot electrons are participating in the reaction. All the results confirm that the hot electron plays a more important role in improving the ENRR activity of the electrocatalyst under illumination. This work provides a very important reference and enlightenment for the effective use of the LSPR effect to improve the catalytic activity of the ENRR electrocatalyst itself.

2. Experimental section

2.1. Materials

Cetyltrimethylammonium bromide (CTAB, 99%), chloroauric acid ($HAuCl_4$, 99.9%), sodium borohydride ($NaBH_4$, 98%), L-ascorbic acid (AA, 99.5%) were purchased from Sigma-Aldrich (Shanghai, China). Silver nitrate ($AgNO_3$, 99.9995%), sodium citrate (Na_3Ct, 99%), salicylic acid, sodium hypochlorite (NaClO, 14.5%), Nafion D-521 (5%, w/w) dispersion solution was obtained from Alfa Aesar. Sodium nitroprusside was supplied by Macklin Inc. Dimethyl sulfoxide was supplied by J&K. Para-(dimethylamino) benzaldehyde (p-$C_9H_{11}NO$), hydrazine monohydrate, ammonium chloride (NH_4Cl), ammonium sulfate $(^{15}NH_4)_2SO_4$ were purchased from Aladdin. Other chemical reagents involving hydrogen peroxide (H_2O_2, 30%), hydrochloric acid (HCl), nitric acid (HNO_3), sodium hydroxide (NaOH), potassium hydroxide (KOH), and ethanol are obtained without further purification and deionized (DI) water is 18.2 MΩ. Carbon paper and Nafion 211 membrane were bought from Toray and DuPont, separately.

2.2. Synthesis of Au NRs

Au NRs were prepared through classic seed-mediated growth method. Firstly, $HAuCl_4$ (0.01 M, 0.25 mL) and freshly prepared $NaBH_4$ solution (0.01 M, 0.6 mL) were successively added into preconfigured CTAB solution (0.1 M, 9.75 mL). After stirring evenly under 600 rpm for 2 min and then keeping undisturbed for 3 h at 35 ℃ water bath, 3–5 nm-sized gold nano-seeds were obtained after centrifugation. Au NRs were then synthesized by adding as-prepared Au seeds (0.1 mL) into a growth solution containing CTAB (0.1 M, 40 mL), $HAuCl_4$ (0.01 M, 2 mL), $AgNO_3$ (0.01 M, 0.4 mL), HCl (1 M, 0.8 mL), and AA (0.1 M, 0.32 mL). The mixed solution was kept at 35 ℃ water bath for at least 6 h before use.

2.3. Preparation of working electrode

The Au NRs working electrode was prepared by the drip coating method. First, the original Au NRs solution was centrifugally cleaned twice and concentrated to achieve a mass concentration of 1.0 mg mL^{-1}. Afterward, 0.1 mL Nafion D-521 dispersion solution was added into 2.0 mL concentrated solution of Au NRs, and the whole solution was uniformly dispersed by ultrasonication for 30 min 0.21 mL of the above mixture was evenly dropped onto the carbon paper (1 cm × 1 cm), and then transferred to a vacuum drying oven and kept at 40 ℃ for 6 h. The resulting carbon paper electrode with Au NRs catalyst was further immersed into anhydrous ethanol to remove the possibly remaining CTAB on the electrode surface.

2.4. Characterization

The morphologies of the samples were characterized by Carl Zeiss SUPRA 55 field-emission scanning electron microscopy (SEM) with an acceleration voltage of 10 kV. The morphologies with higher magnification and lattice stripes of the samples were further observed by Talos F200X transmission electron microscopy (TEM) operated at 200 kV. The mass concentrations of Au NRs were measured using the Aurora M90 inductively coupled plasma atomic emission spectroscopy (ICP-AES). The absorption spectra of the solutions were recorded on a PerkinElmer LAMBDA 750 UV-Vis spectrophotometer.

2.5. Electrochemical measurement

All the electrochemical measurements were performed at room temperature and normal pressure using the CHI 660E electrochemical workstation (Chenhua, Shanghai), where the temperature of the electrolyte (0.1 M KOH) was kept unchanged during the test. In the typical three-electrode system, silver/silver chloride electrode (Ag/AgCl) and Pt electrode were used as reference electrode and counter electrode, respectively. Before the test, the Nafion 211 membrane was pretreated with H_2O_2 (3%) and dilute H_2SO_4 (0.5 M) under 80 ℃ for 1 h, followed by rinsing with DI water for three times, to clean the Nafion membrane for better proton transfer capacity. Highly pure nitrogen (N_2) gas was pumped into the electrolyte for 30 min before testing to remove the dissolved oxygen and to reach a N_2 saturated atmosphere. N_2 gas was continuously flowed in the electrolyte during the data collecting process. All measure potentials were converted to reversible hydrogen potential (vs. RHE) according to the Nernst equation:

$$E(\text{vs.RHE}) = E(\text{vs.Ag/AgCl}) + 0.059 \times \text{pH} + 0.197 \quad (1)$$

In this work, linear sweep voltammetry (LSV) and potentiostatic (*I-t*) measurement methods were applied. The LSV curves were collected at a scan speed of 5 mv s^{-1} with or without the incident illumination, before LSV tests had been performed more than once to make the working electrode stable. *I-t* measurements were conducted under different bias voltages (−0.1, −0.2, −0.3, −0.4, −0.5 V vs. RHE), and the operations under each of the test conditions were carried out more than three times. The lasers used in the test were from Yuanming Ningbo with different wavelengths of 450 nm, 589 nm, 730 nm, 808 nm, and 940 nm. The I_{Rapid}, I_{Slow}, and I_{Total} represent the fast response current, slow response current and total response current under illumination conditions, respectively. The specific calculation formula is: (Scheme S1)

$$I_{Rapid} = |I_1 - I_{on}| \quad (2)$$

$$I_{Slow} = |I_{off} - I_1| \quad (3)$$

$$I_{Total} = |I_{off} - I_{on}| \quad (4)$$

where I_{on} and I_{off} are the current values at the beginning and end of the laser illumination, respectively. I_1 is the current value after 1 s of laser illumination.

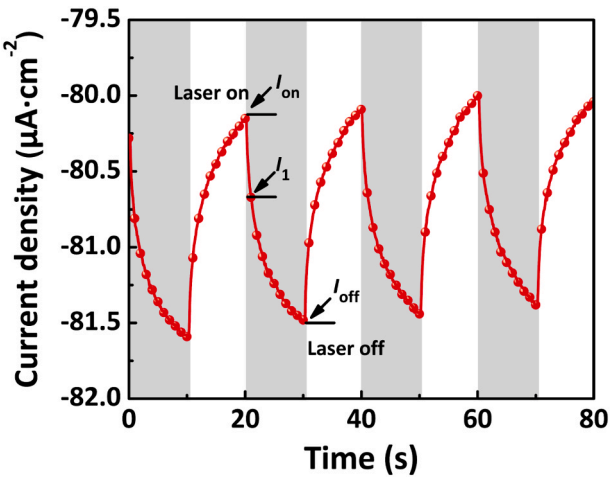

Scheme S1. Schematic illustration of the selection of values that were used to calculate I_{Total}, I_{Rapid}, and I_{Slow} in the Eqs. (2)–(4).

2.6. Detection of ammonia concentration

The mass concentrations of the generated ammonia (NH_3) were detected via an indophenol blue method. In detail, 2 mL electrolyte was mixed with 2 mL NaOH solution (1.0 M) containing 5 wt% salicylic acid and 5 wt% Na_3Ct, followed by the addition of 1 mL NaClO solution (0.05 M) and 0.2 mL sodium nitroprusside (1 wt%). After slight vibration and then incubation in a dark environment for 2 hs, the absorbance of the mixture solution was collected at 655 nm using the UV-Vis spectrophotometer. The standard calibration curve was plotted by testing a series of 0.1 M KOH solutions containing known ammonia concentrations.

2.7. Detection of hydrazine

The amount of the produced hydrazine after the reaction was quantified through Watt and Chrisp's method. Specifically, the color reagent was pre-prepared by dissolving p-$C_9H_{11}NO$ (5.99 g) into the mixed solution of HCl (30 mL) and ethanol (300 mL). 5 mL of the above color reagent was added into 5 mL of the electrolyte, which was then kept for 10 min in dark. Afterward, the absorbance of the resulting solution was acquired at 455 nm using the UV-Vis spectrophotometer. The standard calibration curve used here was plotted by testing a series of KOH solutions (0.1 M) containing known hydrazine concentrations.

2.8. Calculation of ammonia yield rate and Faradaic efficiency

The production yield of NH_3 was obtained according to the following equation:

$$r_{NH_3} = \frac{c_{NH_3} \times V}{t \times A} \quad (5)$$

and the Faradaic efficiency (FE) was calculated by the following equation:

$$FE = \frac{3 \times F \times c_{NH_3} \times V}{Q} \quad (6)$$

where c_{NH_3} is NH_3 concentration (μg mL^{-1}); V, t, and A represent the volume of the electrolyte (mL), reaction time (h), and the actual working area of the working electrode (cm^2), respectively; F is Faraday constant (96485 C mol^{-1}), and Q is the total charge quantity in the electrochemical process.

2.9. Isotope labeling test

The reaction gas was replaced by $^{15}N_2$ for isotope labeling experiments, and the NH_3 product was qualitatively analyzed to determine the source of NH_3. After I-*t*-tests, the pH value of electrolyte solution was adjusted to around 7 by adding H_2SO_4 (0.5 M), which was then concentrated to 5 mL using a rotatory evaporator. After filtration, the pH value of the above solution was further adjusted to 1–2 by adding H_2SO_4 (0.5 M). 0.4 mL of the solution was extracted and mixed evenly with 0.2 mL DMSO-d6, and finally transferred to the NMR tube to conduct ^1H NMR measurements. As for the preparation of the standard sample, a certain amount of $^{14}NH_4Cl$ and $(^{15}NH_4)_2SO_4$ were weighed and dissolved in a 10 mL electrolyte, followed by pH adjustment to 1-2. Similarly, 0.4 mL of the solution was extracted and mixed evenly with 0.2 mL DMSO-d_6, and finally transferred to the NMR tube.

3. Results and discussion

3.1. Preparation and characterization of Au NRs electrode

The preparation procedure of Au NRs-based electrode and the design of LSPR enhanced ENRR are shown in Fig. 1a and b. The concentrated Au NRs-naphthol mixture was dropped onto the surface of carbon paper, scraped evenly, and dried in vacuum to obtain Au NRs electrode. Under the illumination conditions, the LSPR effect of Au NRs can further enhance the ENRR activity of itself (Fig. 1b). Almost no other shapes of Au are observed in the scanning electron microscopy (SEM) image in Fig. S1, indicating that Au NRs were synthesized with high yield and had a uniform morphology and size. The length of the Au NRs is about 60 nm and the diameter is about 16 nm as observed from the transmission electron microscopy (TEM) image in Fig. 1c. The high-resolution TEM (HRTEM) image reveals that the Au NRs are single crystals and the nanorods grow along the [100] direction (Fig. 1d) [44–46]. The SEM images of Au NRs electrode are shown in Fig. 1e, it can be seen that Au NRs are relatively uniformly dispersed on the surface of carbon paper. The X-Ray diffraction (XRD) results of Au NRs electrode and blank carbon paper are shown in Fig. S2. The intense peaks located at 38.18°, 44.39°, and 46.58° are indexed to (111), (200), and (220) planes of Au (JCPDS no. 04–0784), respectively. The extra peaks located at 43.00° and 54.43° belong to the carbon paper. The results of ultraviolet-visible (UV-Vis) spectra also prove this conclusion, as shown in Fig. 1f. Au NRs exhibit two peaks at 512 nm and 756 nm, which are due to the transverse plasmonic resonance and longitudinal plasmonic resonance, respectively [44]. Compared with Au NRs, the extinction spectrum of Au NRs electrode did not change too much, where only slight red shift and broadening were observed, possibly due to the change of the medium environment and the slight accumulation of Au NRs. Therefore, the special electrode preparation method effectively ensures the relatively uniform dispersion of Au NRs on the surface of carbon paper, thus avoiding the reduction of catalytic active sites caused by nanoparticle agglomeration and basically maintaining the LSPR property of Au NRs.

3.2. ENRR analysis under illumination

To determine the influence of the LSPR effect of Au NRs on its NRR activity under illumination conditions, the NRR of Au NRs electrode was measured in the presence/absence of illumination in an airtight double-chamber electrochemical cell with a quartz window on the side separated by Nafion 211 membrane, and the electrolyte is KOH solution (0.1 M), as shown in Fig. 1a. The linear sweep voltammetry (LSV) curves were conducted under dark conditions to estimate the NRR activity of Au NRs in N_2-saturated and Ar-saturated electrolyte solution (Fig. 2a, dotted line). The LSV curves under different gas atmospheres show the analogous trend but different current densities. In the potential range of - 0.05 ~ - 0.65 V, the current density of N_2-saturated solution is significantly higher than that of inert Ar-saturated solution, which

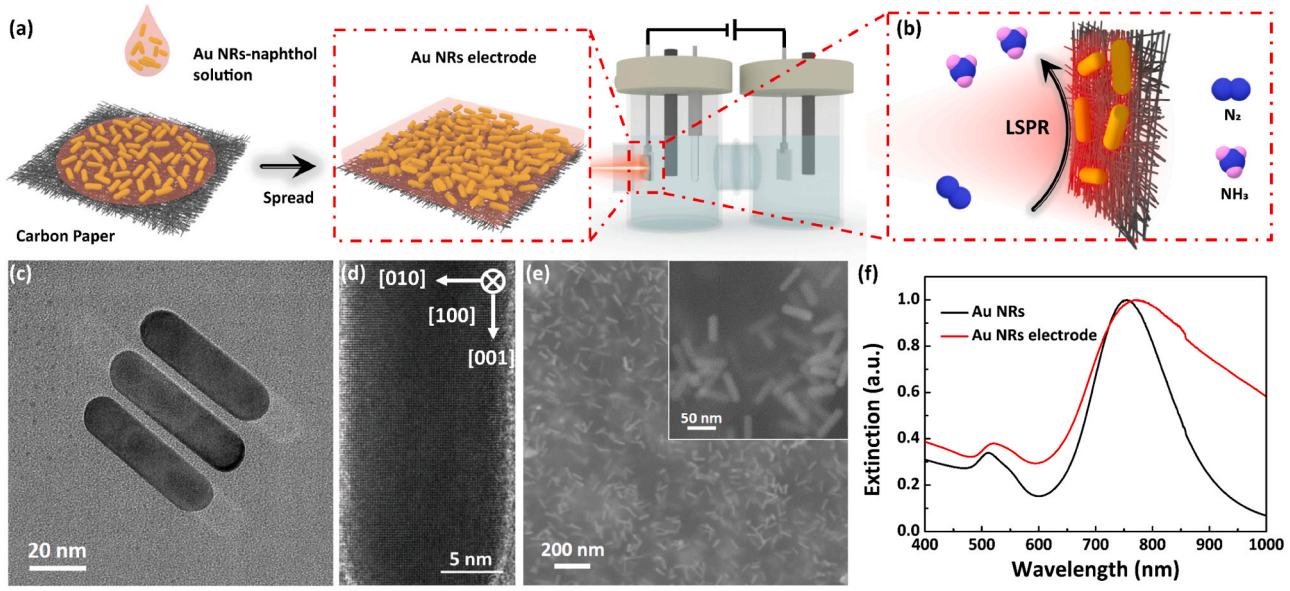

Fig. 1. (a) Schematic illustration of the fabrication of the Au NRs electrode; (b) Schematic diagram of the LSPR enhanced ENRR; (c) TEM image of the Au NRs; (d) HRTEM image of the Au NRs; (e) SEM image of Au NRs electrode; (f) the extinction spectra of Au NRs (black) and Au NRs electrode (red). (For interpretation of the references to colour in this figure legend, the reader is referred to the web version of this article.)

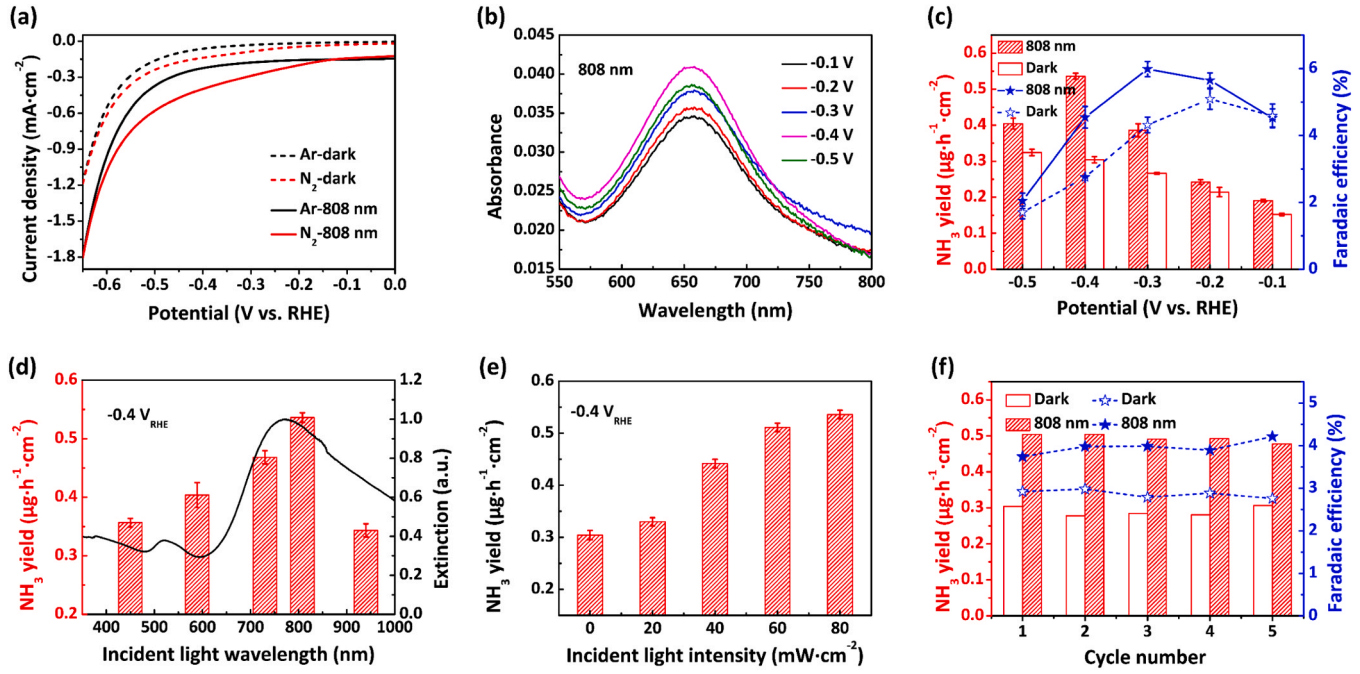

Fig. 2. (a) LSV curves of Au NRs electrode in an Ar (black) and N_2 (red) saturated environment under dark (dotted line) and 808 nm laser illumination (solid line) conditions; (b) the UV-Vis absorption spectra of NH_3 formation at selected potentials (808 nm). (c) ammonia yield rate and FE at various potentials under dark (blank column) and 808 nm laser illumination (red column) conditions; (d) comparison of the extinction spectrum of Au NRs (black line) and the ammonia yield rate under different wavelength conditions (red column); (e) the ammonia yield rate of Au NRs electrode under different laser intensities; (f) cycling stability results of ammonia yield rate on Au NRs electrode under dark (blank column) and 808 nm laser illumination (red column) conditions. Each cycle test was carried out at − 0.4 V vs. RHE in 0.1 M KOH at 20 °C. (For interpretation of the references to colour in this figure legend, the reader is referred to the web version of this article.)

preliminarily proves that Au NRs have a good ENRR activity. Under 808 nm laser illumination (80 mW cm^{-2}), the current density of N_2-saturated and Ar-saturated solution both showed a certain increase (Fig. 2a, solid line). It is worth noting that, compared with dark conditions, the current density of N_2-saturated solution under laser illumination presents a greater increase than that of Ar-saturated solution, indicating that the catalytic activity of Au NRs in the potential range of − 0.05 ~ − 0.65 V could be effectively improved under the illumination. The NRR performance of Au NRs electrode and the enhancement effect of illumination were further estimated by chronoamperometry tests. The concentration of ammonia was measured using the indophenol blue method and the colorimetric calibration curve results of NH_3 and hydrazine (N_2H_4) are shown in the Figs. S3 and S4. The ammonia yield rate and FE at different potentials are plotted in Fig. 2c. No N_2H_4 was detected at each given potential under dark or illumination condition (Fig. S5). Within the potential range of − 0.1 V to

− 0.5 V, the ammonia yield rate increases with the negative potential to − 0.5 V and reaches the maximum (0.33 μg h^{-1} cm^{-2}), and the FE reaches the maximum at − 0.3 V in dark. With laser irradiation, the ammonia yield rate of Au NRs electrode has been greatly improved. Fig. 2b showed the UV-Vis absorption spectra of NH_3 formation at selected potentials (808 nm) and the ammonia yield rate reaches the maximum of 0.54 μg h^{-1} cm^{-2} at − 0.4 V, which is about 63.6% higher than the yield rate in dark (details are shown in Figs. S6 and S7). To exclude the influence of the photocatalytic NRR activity of the Au NRs electrode on the test results, the ammonia yield rate of Au NRs electrode under laser irradiation (808 nm, 80 mW cm^{-2}) without applied potential was further explored. As shown in Fig. S8, the resultant ammonia yield rate is far lower than that in ENRR. All the results further prove that the illumination can effectively enhance the ENRR activity of Au NRs electrode.

To determine the improvement of ENRR performance of Au NRs electrode under the illumination condition is caused by the LSPR effect, the ammonia yield rates under laser irradiation with different wavelengths were further explored (Fig. S9). The laser power of all wavelengths was maintained at 80 mW cm^{-2} and the ammonia yield rate was compared at − 0.4 V potential. As shown in Fig. 2d, Au NRs electrode exhibits different NRR activities under different wavelength irradiation and exhibits the highest ammonia yield rate with 808 nm laser illumination. The trend of the NRR activity of Au NRs electrode relative to wavelength is consistent with the extinction spectrum, indicating the increase of NRR activity of Au NRs electrode under illumination is caused by the LSPR effect of Au NRs [24]. Meanwhile, Fig. 2e demonstrates the NRR activity of Au NRs under different laser intensities. The ammonia yield rate shows a strong dependence on the light intensity, which further proves the above conclusion (Fig. S10) [20,22]. In addition, the durability of Au NRS electrode was further investigated. During 5 consecutive electrolysis cycles, the current density of Au NRs electrode does not change significantly with illumination (Fig. S11). More importantly, the ammonia yield rate and FE of Au NRs electrode under illumination conditions still maintain excellent NRR activity enhancement stability after 5 recycling tests, as shown in Fig. 2f. The morphology of Au NRs electrode after 5 consecutive electrolysis cycles is characterized by SEM (Fig. S12), and there is basically no change compared with the fresh electrode (Fig. 1e), which proves the Au NRs electrode has good structural stability. During the test, no detectable NH_3 was produced when the Ar-saturated electrolyte solution or blank carbon paper was used as a control experiment (Fig. S13). The ^{15}N isotope labeling experiment further confirmed that the NH_3 detected under standard conditions was obtained from the catalytic conversion of the N_2 in the electrolyte solution by the Au NRs electrode (Fig. S14) [47,48]. In addition, the NOx contaminants in the N_2 could affect the accuracy of the experimental results and the ammonia yield rate under the N_2 after NO_x removal is about 0.31 μg h^{-1} cm^{-2}, which is about 94% of the ammonia yield rate of untreated N_2 [49,50]. After NO_x removal, the LSPR effect also showed similar ammonia yield improvement ability. (Fig. S15). The results prove the NOx contaminants will not significantly affect the conclusion that LSPR effect can effectively improve the ENRR catalytic activity of Au NRs.

3.3. Theoretical investigation

Furthermore, the Finite difference time domain method (FDTD) was used to simulate the electromagnetic field intensity and current density distribution of Au NRs at different wavelengths to explore the reasons for the enhancement of the electrocatalytic activity of NRR under the illumination conditions. Fig. S16 shows the simulated extinction spectra of single Au NRs with longitudinal peaks at 756 nm, which is basically consistent with the experimental results. The electromagnetic field distributions of Au NRs at different wavelengths are shown in Fig. 3a and the strongest electromagnetic field is concentrated on both ends of the Au NRs with 808 nm irradiation. Fig. S17 summarizes the average electromagnetic field intensity of Au NRs under different wavelengths of illumination, and the trend is consistent with the extinction spectrum change. The higher intense of extinction, the more intense the LSPR effect of Au NRs and the stronger the electromagnetic field generated. The current density distributions of Au NRs at different wavelengths are shown in the Fig. 3b. The trend of current density versus wavelength is consistent with that of electromagnetic field intensity and the surface of Au NRs exhibits the largest current density under 808 nm, indicating that more energetic charge carriers (e-h pairs) are formed at this wavelength [20,51]. The strength of electromagnetic field directly determines the number of hot electrons generated by Au NRs under illumination conditions. Thus, based on the LSPR effect, the surface of Au NRs can generate a stronger electromagnetic field and further decays to

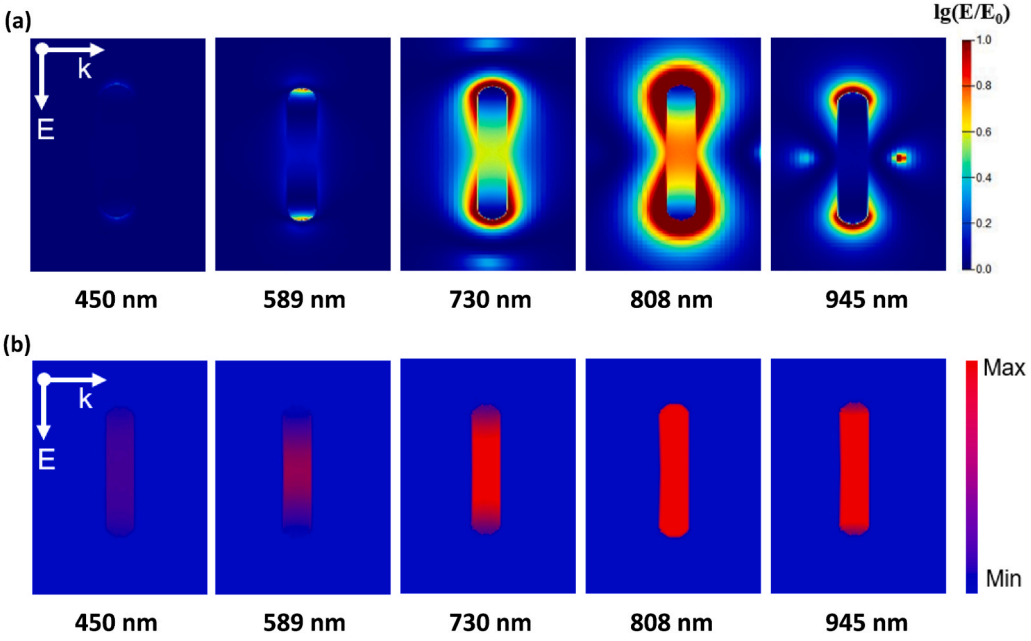

Fig. 3. (a) The electromagnetic field distribution of Au NRs at different wavelengths (450, 589, 730, 808, and 945 nm); (b) the current density distribution of Au NRs at different wavelengths (450, 589, 730, 808, and 945 nm).

generate more high-energy hot electrons under the optimal wavelength illumination condition (808 nm), which is the main reason for achieving the enhancement of ENRR activity of Au NRs electrode.

3.4. Photocurrent investigation

To determine the specific mechanism of the enhanced ENRR activity of Au NRs electrode by LSPR effect with illumination, the photocurrent of the Au NRs electrode under different laser wavelength conditions were further explored. Fig. 4a depicts the on-off photocurrent density curve of the Au NRs electrode with 808 nm laser at − 0.4 V potential. The photocurrent is composed of two different regions: the rapid-response current (I_{Rapid}) and the slow-response current (I_{Slow}). During plasmon-mediated chemical reactions, plasmon relaxations can be divided into two simultaneous processes: hot electron injection and photoheating [52]. The photocurrent generated by hot electron injection responds to light irradiation in milliseconds, whereas the photothermal effect is much slower. Hence, the rapid-response current (I_{Rapid}) can be related to the plasmon hot electron and the slow-response current (I_{Slow}) can be related to the photothermal effects, respectively. (the detail in Experimental section for the extraction process of I_{Rapid}, I_{Slow}, and I_{Total}) [52,53]. Fig. S18 shows the photocurrent of the blank carbon paper under the irradiation of 808 nm laser (80 mW cm^{-2}) and there is no obvious current change, indicating that the photo-response current is caused by the LSPR effect of Au NRs electrode. The photocurrent density curves of Au NRs electrode at different wavelengths were further analyzed and compared (Fig. 4b). As shown in Fig. 4c, the Au NRs electrode exhibits different I_{Rapid} responses under different wavelengths, and the changing trend is consistent with the extinction spectrum, which reaches the maximum under the irradiation of 808 nm laser. Meanwhile, the ratio of the I_{Rapid} to the total response photocurrent (I_{Total}, I_{Rapid}/I_{Total}) also reaches the maximum value under the condition of 808 nm laser, implying more hot electrons contribute to the improvement of photocurrent density under this wavelength (Fig. 4c, red line). Combined with the results of FDTD, the LSPR effect of Au NRs is the strongest at 808 nm, which can excite the largest electromagnetic field, so that more high-energy hot electrons can be generated and effectively improving the electrocatalytic activity of Au NRs. Fig. 4d shows the photocurrent density of the Au NRs electrode under different 808 nm laser intensity conditions. As the laser intensity increases, the I_{Rapid} and the I_{Total} gradually augment. It is worth noting that the I_{Rapid}/I_{Total} has a linear relationship with the laser intensity, indicating that the higher the incident light intensity is, the stronger the LSPR is generated and the more hot electrons are excited accordingly (Fig. 4e). At the same time, the greater the ratio of I_{Rapid}/I_{Total}, the higher the final ammonia yield rate, indicating that the hot electrons generated by the LSPR effect are the main contribution for the effective improvement of the ENRR efficiency of Au NRs under the illumination (Fig. S19). Finally, the average increase ratios of the different products under illumination ($r_{Light-Dark}/r_{Dark}$) were further compared, where r_{Light} is the average yield rate under illumination and r_{Dark} is the average yield rate in dark. As shown in Fig. 4f, the yield rate of hydrogen increased by about 17.0% and the ammonia yield rate increased by about 63.6% after illumination, indicating that hot electrons excited by the LSPR effect of Au NRs can effectively promote ENRR. It is well known that Au does not exhibit a good HER catalytic activity and it is not an ideal catalytic material for HER [54]. On the contrary, Au exhibits a preferable ENRR activity, making it a relatively good ENRR catalytic material [55]. The ENRR enhancement of Au NRs by illumination is greater than the HER enhancement, probably because Au is a better catalytic material for ENRR than HER.

4. Conclusion

In summary, we successfully achieved an effective enhancement of the electrocatalytic NRR activity of Au NRs under illumination based on the LSPR effect. The drip-coating method of electrode preparation effectively avoids the aggregation of nanoparticles and maintains the LSPR properties of Au NRs. Under the condition of 808 nm laser (80 mW cm^{-2}), the ammonia yield rate of Au NRs was increased by about

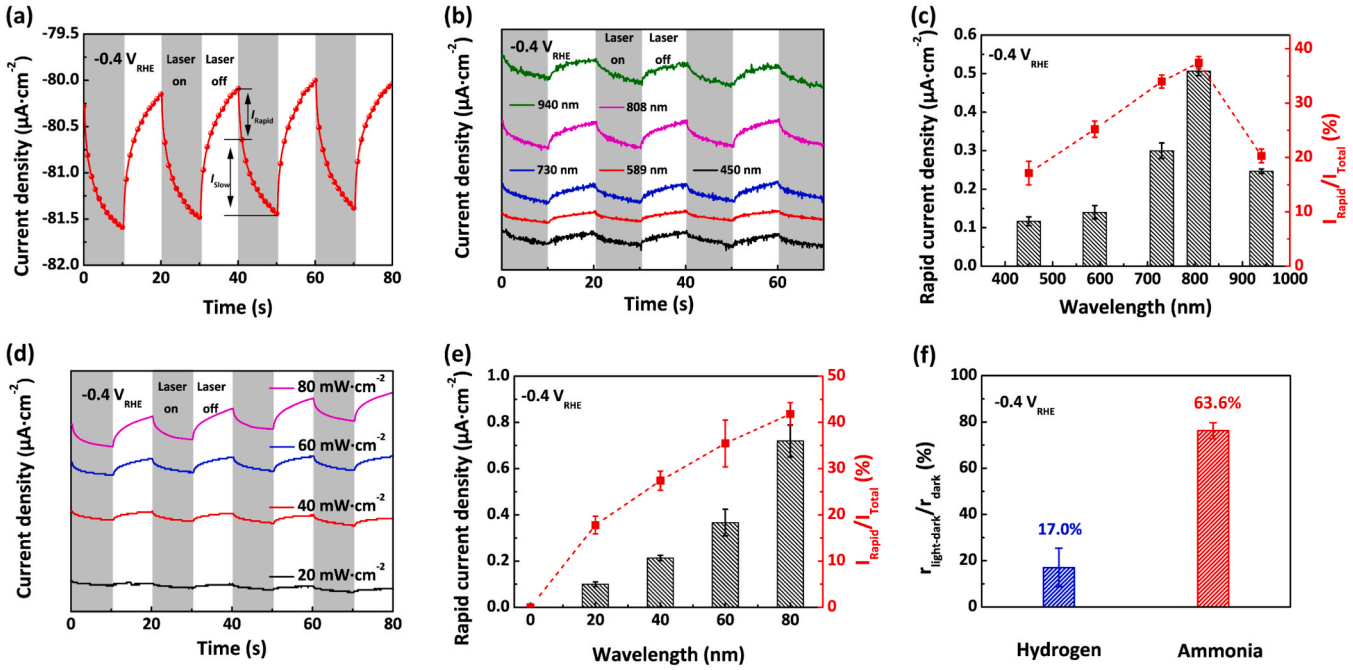

Fig. 4. (a) The on-off photocurrent density of the Au NRs electrode with 808 nm laser under − 0.4 V potential; (b) the current density-time curves of Au NRs electrode at different wavelengths; (c) the rapid-response current density (black column) and the ratio of the I_{Rapid} to the I_{Total} at different wavelengths; (d) the current density-time curves of Au NRs electrode at different intensity of 808 nm laser; (e) the rapid-response current density (black column) and the ratio of the I_{Rapid} to the I_{Total} at different laser intensities; (f) the average increase ratio ($r_{light-dark}/r_{dark}$) of all products obtained from the electrocatalytic reaction of Au NRs electrode under the illumination. (For interpretation of the references to colour in this figure legend, the reader is referred to the web version of this article.)

63.6% compared with that in dark. The results of FDTD simulation and photocurrent analysis further prove that the hot electrons generated by LSPR effect can effectively promote the catalytic activity of ENRR and improve the ammonia yield rate. This work opens a new direction for the design and development of novel LSPR-enhanced electrocatalysts for NRR in the future.

Author Contributions

The manuscript was written through contributions of all authors. All authors have given approval to the final version of the manuscript.

CRediT authorship contribution statement

Wenkai Liang: Conceptualization, Methodology, Validation, Data curation, Writing – original draft. **Wei Qin:** Investigation, Formal analysis, Data curation. **Dong Li:** Software, Formal analysis, Data curation. **Yawen Wang:** Investigation, Writing – review & editing. **Wei Guo:** Visualization, Formal analysis. **Yuanting Bi:** Investigation. **Yinghui Sun:** Validation, Visualization, Supervision, Writing – review & editing. **Lin Jiang:** Conceptualization, Methodology, Writing – review & editing, Resources, Supervision, Project administration, Funding acquisition.

Declaration of Competing Interest

The authors declare that they have no known competing financial interests or personal relationships that could have appeared to influence the work reported in this paper.

Acknowledgment

This work was financially supported by grants from the National Natural Science Foundation of China (21822202 and 22072104), the National Key R&D Program of China (International Collaboration program) granted by Chinese Ministry of Science and Technology (2018YFE0200700). This is also a project funded by Suzhou Key Laboratory of Functional Nano & Soft Materials, Collaborative Innovation Center of Suzhou Nano Science and Technology, the 111 project, and Joint International Research Laboratory of Carbon-Based Functional Materials and Devices.

Appendix A. Supporting information

Supplementary data associated with this article can be found in the online version at doi:10.1016/j.apcatb.2021.120808.

References

[1] L. Zhou, J.M.P. Martirez, J. Finzel, C. Zhang, D.F. Swearer, S. Tian, H. Robatjazi, M. Lou, L. Dong, L. Henderson, P. Christopher, E.A. Carter, P. Nordlander, N. J. Halas, Light-driven methane dry reforming with single atomic site antenna-reactor plasmonic photocatalysts, Nat. Energy 5 (2020) 61–70.
[2] M.-Q. Yang, Y.-J. Xu, W. Lu, K. Zeng, H. Zhu, Q.-H. Xu, G.W. Ho, Self-surface charge exfoliation and electrostatically coordinated 2D hetero-layered hybrids, Nat. Commun. 8 (2017) 14224.
[3] Y. Yan, R.W. Crisp, J. Gu, B.D. Chernomordik, G.F. Pach, A.R. Marshall, J. A. Turner, M.C. Beard, Multiple exciton generation for photoelectrochemical hydrogen evolution reactions with quantum yields exceeding 100%, Nat. Energy 2 (2017) 17052.
[4] S. Chen, T. Takata, K. Domen, Particulate photocatalysts for overall water splitting, Nat. Rev. Mater. 2 (2017) 17050.
[5] N. Armaroli, V. Balzani, The future of energy supply: challenges and opportunities, Angew. Chem. Int. Ed. 46 (2007) 52–66.
[6] L. Zhou, D.F. Swearer, C. Zhang, H. Robatjazi, H. Zhao, L. Henderson, L. Dong, P. Christopher, E.A. Carter, P. Nordlander, N.J. Halas, Quantifying hot carrier and thermal contributions in plasmonic photocatalysis, Science 362 (2018) 69–72.
[7] C. Zhan, X.-J. Chen, J. Yi, J.-F. Li, D.-Y. Wu, Z.-Q. Tian, From plasmon-enhanced molecular spectroscopy to plasmon-mediated chemical reactions, Nat. Rev. Chem. 2 (2018) 216–230.
[8] X.J. Zeng, Y. Zhao, X.D. Hu, G.D. Stucky, M. Moskovits, Rational component and structure design of noble-metal composites for optical and catalytic applications, Small Struct. 2 (2021), 2000138.
[9] S. Wang, L. Chen, X. Zhao, J. Zhang, Z. Ao, W. Liu, H. Wu, L. Shi, Y. Yin, X. Xu, C. Zhao, X. Duan, S. Wang, H. Sun, Efficient photocatalytic overall water splitting on metal-free 1D SWCNT/2D ultrathin C3N4 heterojunctions via novel non-resonant plasmonic effect, Appl. Catal. B-Environ. 278 (2020), 119312.
[10] A. Manjavacas, J.G. Liu, V. Kulkarni, P. Nordlander, Plasmon-induced hot carriers in metallic nanoparticles, ACS Nano 8 (2014) 7630–7638.
[11] S. Linic, U. Aslam, C. Boerigter, M. Morabito, Photochemical transformations on plasmonic metal nanoparticles, Nat. Mater. 14 (2015) 567–576.
[12] Y. Li, J.-G. Wang, Y. Fan, H. Sun, W. Hua, H. Liu, B. Wei, Plasmonic TiN boosting nitrogen-doped TiO2 for ultrahigh efficient photoelectrochemical oxygen evolution, Appl. Catal. B-Environ. 246 (2019) 21–29.
[13] S. Mukherjee, F. Libisch, N. Large, O. Neumann, L.V. Brown, J. Cheng, J.B. Lassiter, E.A. Carter, P. Nordlander, N.J. Halas, Hot electrons do the impossible: plasmon-induced dissociation of H_2 on Au, Nano Lett. 13 (2013) 240–247.
[14] C. Hu, X. Chen, J. Jin, Y. Han, S. Chen, H. Ju, J. Cai, Y. Qiu, C. Gao, C. Wang, Z. Qi, R. Long, L. Song, Z. Liu, Y. Xiong, Surface plasmon enabling nitrogen fixation in pure water through a dissociative mechanism under mild conditions, J. Am. Chem. Soc. 141 (2019) 7807–7814.
[15] T. Hou, L. Chen, Y. Xin, W. Zhu, C. Zhang, W. Zhang, S. Liang, L. Wang, Porous CuFe for plasmon-assisted N_2 photofixation, ACS Energy Lett. 5 (2020) 2444–2451.
[16] H. Yang, L.-Q. He, Y.-W. Hu, X. Lu, G.-R. Li, B. Liu, B. Ren, Y. Tong, P.-P. Fang, Quantitative detection of photothermal and photoelectrocatalytic effects induced by SPR from Au@Pt nanoparticles, Angew. Chem. Int. Ed. 54 (2015) 11462–11466.
[17] M. Tahir, B. Tahir, N.A.S. Amin, Synergistic effect in plasmonic Au/Ag alloy NPs co-coated TiO_2 NWs toward visible-light enhanced CO_2 photoreduction to fuels, Appl. Catal. B-Environ. 204 (2017) 548–560.
[18] S. Sun, Q. An, M. Watanabe, J. Cheng, H.H. Kim, T. Akbay, A. Takagaki, T. Ishihara, Highly correlation of CO_2 reduction selectivity and surface electron Accumulation: a case study of Au-MoS_2 and Ag-MoS_2 catalyst, Appl. Catal. B-Environ. 271 (2020), 118931.
[19] M.L. Brongersma, N.J. Halas, P. Nordlander, Plasmon-induced hot carrier science and technology, Nat. Nanotechnol. 10 (2015) 25–34.
[20] U. Aslam, S. Chavez, S. Linic, Controlling energy flow in multimetallic nanostructures for plasmonic catalysis, Nat. Nanotechnol. 12 (2017) 1000–1005.
[21] C. Zhang, H. Zhao, L. Zhou, A.E. Schlather, L. Dong, M.J. McClain, D.F. Swearer, P. Nordlander, N.J. Halas, Al-Pd nanodisk heterodimers as antenna-reactor photocatalysts, Nano Lett. 16 (2016) 6677–6682.
[22] S.K. So, R. Franchy, W. Ho, Photodesorption of NO from Ag(111) and Cu(111), J. Chem. Phys. 95 (1991) 1385–1399.
[23] T. Peng, J. Miao, Z. Gao, L. Zhang, Y. Gao, C. Fan, D. Li, Reactivating catalytic surface: insights into the role of hot holes in plasmonic catalysis, Small 14 (2018), 1703510.
[24] M.J. Kale, T. Avanesian, H. Xin, J. Yan, P. Christopher, Controlling catalytic selectivity on metal nanoparticles by direct photoexcitation of adsorbate-metal bonds, Nano Lett. 14 (2014) 5405–5412.
[25] Z. Wang, J. Du, Y. Zhang, J. Han, S. Huang, A. Hirata, M. Chen, Free-standing nanoporous gold for direct plasmon enhanced electrooxidation of alcohol molecules, Nano Energy 56 (2019) 286–293.
[26] S.-C. Lin, C.-S. Hsu, S.-Y. Chiu, T.-Y. Liao, H.M. Chen, Edgeless Ag-Pt bimetallic nanocages: in situ monitor plasmon-induced suppression of hydrogen peroxide formation, J. Am. Chem. Soc. 139 (2017) 2224–2233.
[27] L. Huang, J. Zou, J.-Y. Ye, Z.-Y. Zhou, Z. Lin, X. Kang, P.K. Jain, S. Chen, Synergy between plasmonic and electrocatalytic activation of methanol oxidation on palladium-silver alloy nanotubes, Angew. Chem. Int. Ed. 58 (2019) 8794–8798.
[28] E.B. Creel, E.R. Corson, J. Eichhorn, R. Kostecki, J.J. Urban, B.D. McCloskey, Directing selectivity of electrochemical carbon dioxide reduction using plasmonics, ACS Energy Lett. 4 (2019) 1098–1105.
[29] J. Zheng, Y. Lyu, M. Qiao, J.P. Veder, R.D. Marco, J. Bradley, R. Wang, Y. Li, A. Huang, S.P. Jiang, S. Wang, Tuning the electron localization of gold enables the control of nitrogen-to-ammonia fixation, Angew. Chem. Int. Ed. 58 (2019) 18604–18609.
[30] F. Wang, L.M. Mao, H.T. Xie, J. Mao, Graphene derivatives and graphene composite electrocatalysts for N_2 reduction reaction, Small Struct. 2 (2021), 2000075.
[31] Y.-J. Shih, Z.-L. Wu, C.-Y. Lin, Y.-H. Huang, C.-P. Huang, Manipulating the crystalline morphology and facet orientation of copper and copper-palladium nanocatalysts supported on stainless steel mesh with the aid of cationic surfactant to improve the electrochemical reduction of nitrate and N2 selectivity, Appl. Catal. B-Environ. 273 (2020), 119053.
[32] M. Falcone, L. Chatelain, R. Scopelliti, I. Zivkovic, M. Mazzanti, Nitrogen reduction and functionalization by a multimetallic uranium nitride complex, Nature 547 (2017) 332–335.
[33] K.A. Brown, D.F. Harris, M.B. Wilker, A. Rasmussen, N. Khadka, H. Hamby, S. Keable, G. Dukovic, J.W. Peters, L.C. Seefeldt, P.W. King, Light-driven dinitrogen reduction catalyzed by a CdS: nitrogenase MoFe protein biohybrid, Science 352 (2016) 448–450.
[34] J.S. Anderson, J. Rittle, J.C. Peters, Catalytic conversion of nitrogen to ammonia by an iron model complex, Nature 501 (2013) 84–87.
[35] X. Wang, S. Qiu, J. Feng, Y. Tong, F. Zhou, Q. Li, L. Song, S. Chen, P. Su, S. Ye, F. Hou, S.X. Dou, H.K. Liu, G.Q. Lu, C. Sun, J. Liu, J. Liang, K.-H. Wu, Confined Fe-Cu clusters as sub-nanometer reactors for efficiently regulating the electrochemical nitrogen reduction reaction, Adv. Mater. 32 (2020), 2004382.

[36] L. Han, Z. Ren, P. Ou, H. Cheng, N. Rui, L. Lin, X. Liu, L. Zhuo, J. Song, J. Sun, J. Luo, H.L. Xin, Modulating single-atom palladium sites with copper for enhanced ambient ammonia electrosynthesis, Angew. Chem. Int. Ed. 60 (2021) 345–350.
[37] D. Bao, Q. Zhang, F.-L. Meng, H.-X. Zhong, M.-M. Shi, Y. Zhang, J.-M. Yan, Q. Jiang, X.-B. Zhang, Electrochemical reduction of N_2 under ambient conditions for artificial N_2 fixation and renewable energy storage using N_2/NH_3 cycle, Adv. Mater. 29 (2017), 1604799.
[38] Y.-C. Hao, Y. Guo, L.-W. Chen, M. Shu, X.-Y. Wang, T.-A. Bu, W.-Y. Gao, N. Zhang, X. Su, X. Feng, J.-W. Zhou, B. Wang, C.-W. Hu, A.-X. Yin, R. Si, Y.-W. Zhang, C.-H. Yan, Promoting nitrogen electroreduction to ammonia with bismuth nanocrystals and potassium cations in water, Nat. Catal. 2 (2019) 448–456.
[39] C. Ling, Y. Zhang, Q. Li, X. Bai, L. Shi, J. Wang, New mechanism for N_2 reduction: the essential role of surface hydrogenation, J. Am. Chem. Soc. 141 (2019) 18264–18270.
[40] Y. Yao, H. Wang, X.-z Yuan, H. Li, M. Shao, Electrochemical nitrogen reduction reaction on ruthenium, ACS Energy Lett. 4 (2019) 1336–1341.
[41] L. Wang, M. Xia, H. Wang, K. Huang, C. Qian, C.T. Maravelias, G.A. Ozin, Greening ammonia toward the solar ammonia refinery, Joule 2 (2018) 1055–1074.
[42] Z.J. Schiffer, K. Manthiram, Electrification and decarbonization of the chemical industry, Joule 1 (2017) 10–14.
[43] M. Nazemi, M.A. El-Sayed, Plasmon-enhanced photo(electro)chemical nitrogen fixation under ambient conditions using visible light responsive hybrid hollow Au-Ag_2O nanocages, Nano Energy 63 (2019), 103886.
[44] H. Jia, A. Du, H. Zhang, J. Yang, R. Jiang, J. Wang, C.-y Zhang, Site-selective growth of crystalline ceria with oxygen vacancies on gold nanocrystals for near-infrared nitrogen photofixation, J. Am. Chem. Soc. 141 (2019) 5083–5086.
[45] C.K. Tsung, X.S. Kou, Q.H. Shi, J.P. Zhang, M.H. Yeung, J.F. Wang, G.D. Stucky, Selective shortening of single-crystalline gold nanorods by mild oxidation, J. Am. Chem. Soc. 128 (2006) 5352–5353.
[46] M.Z. Liu, P. Guyot-Sionnest, Mechanism of silver(I)-assisted growth of gold nanorods and bipyramids, J. Phys. Chem. B 109 (2005) 22192–22200.
[47] Y. Yang, S.-Q. Wang, H. Wen, T. Ye, J. Chen, C.-P. Li, M. Du, Nanoporous gold embedded ZIF composite for enhanced electrochemical nitrogen fixation, Angew. Chem. Int. Ed. 58 (2019) 15362–15366.
[48] Y.-X. Lin, S.-N. Zhang, Z.-H. Xue, J.-J. Zhang, H. Su, T.-J. Zhao, G.-Y. Zhai, X.-H. Li, M. Antonietti, J.-S. Chen, Boosting selective nitrogen reduction to ammonia on electron-deficient copper nanoparticles, Nat. Commun. 10 (2019) 4380.
[49] J. Choi, B.H.R. Suryanto, D. Wang, H.-L. Du, R.Y. Hodgetts, F.M.F. Vallana, D. R. MacFarlane, A.N. Simonov, Identification and elimination of false positives in electrochemical nitrogen reduction studies, Nat. Commun. 11 (2020) 5546.
[50] Y. Chen, H. Liu, N. Ha, S. Licht, S. Gu, W. Li, Revealing nitrogen-containing species in commercial catalysts used for ammonia electrosynthesis, Nat. Catal. 3 (2020) 1055–1061.
[51] T.H. Chow, Y. Lai, X. Cui, W. Lu, X. Zhuo, J. Wang, Colloidal gold nanorings and their plasmon coupling with gold nanospheres, Small 15 (2019), 1902608.
[52] W. Ou, B. Zhou, J. Shen, T.W. Lo, D. Lei, S. Li, J. Zhong, Y.Y. Li, J. Lu, Thermal and nonthermal effects in plasmon-mediated electrochemistry at nanostructured Ag electrode, Angew. Chem. Int. Ed. 59 (2020) 6790–6793.
[53] C. Zhan, B.-W. Liu, Y.-F. Huang, S. Hu, B. Ren, M. Moskovits, Z.-Q. Tian, Disentangling charge carrier from photothermal effects in plasmonic metal nanostructures, Nat. Commun. 10 (2019) 2671.
[54] Y. Zheng, Y. Jiao, Y. Zhu, L.H. Li, Y. Han, Y. Chen, A. Du, M. Jaroniec, S.Z. Qiao, Hydrogen evolution by a metal-free electrocatalyst, Nat. Commun. 5 (2014) 3783.
[55] W. Guo, K. Zhang, Z. Liang, R. Zou, Q. Xu, Electrochemical nitrogen fixation and utilization: theories, advanced catalyst materials and system design, Chem. Soc. Rev. 48 (2019) 5658–5716.